Graphene Oxide Exacerbates Dextran Sodium Sulfate-Induced Colitis via ROS/AMPK/p53 Signaling to Mediate Apoptosis

Siliang Liu
Southern Medical University
Angao Xu
Huizhou Medicine Institute
Yue Xie
Southern Medical University
Zhipeng Liu
Southern Medical University
Meiling Sun
Southern Medical University
Yanfei Gao
Southern Medical University
Hua Mao
Southern Medical University
Xinying Wang (helenwxy@smu.edu.cn)

Research

Keywords: Graphene oxide, Colitis, Intestinal epithelial cell, Apoptosis, Reactive oxygen species, AMP-activated protein kinase (AMPK)

Posted Date: July 9th, 2020

DOI: https://doi.org/10.21203/rs.3.rs-38975/v1

Version of Record: A version of this preprint was published on March 25th, 2021. See the published version at https://doi.org/10.1186/s12951-021-00832-5.

Abstract

Background: Graphene oxide (GO), a novel carbon-based nanomaterial, has immense utility in biomedicine. However, it exerts potential cytotoxic effects on the cells of the gastrointestinal tract (GI), although the underlying mechanisms remain largely uncharacterized. We investigated the potential toxic effect of GO in the intestinal tract under pre-existing inflammatory conditions, such as inflammatory bowel disease (IBD), and elucidated these mechanisms.

Results: Our findings indicated that oral gavage of GO worsened acute colitis induced by 2.5% dextran sodium sulfate (DSS) in mice. *In vitro*, the uptake of GO resulted in decreased cell viability, as well as elevated release of lactic dehydrogenase (LDH) in intestinal epithelial cells (IECs). Moreover, IECs exposed to GO treatment triggered apoptosis through activation of reactive oxygen species (ROS)/AMPK/p53 pathway, as evidenced by the upregulation of cytochrome c (Cytc), Bax, cleaved caspase-3, and the downregulation of Bcl-2. Interestingly, pretreatment with an antioxidant, N-acetyl-L-cysteine (NAC), and a specific inhibitor of AMPK activation, Compound C, effectively inhibited GO-induced apoptosis.

Conclusions: Our data demonstrate that GO aggravated DSS-induced acute colitis in mice could involve GO-induced IEC apoptosis via activation of the ROS/AMPK/p53 pathway. These findings provide a new insight into the pathogenesis of IBD induced by environmental factors and enhance our understanding of GO as an environmental toxin. This study demonstrates the cytotoxic effect exerted by environmental toxins such as GO and its derivatives, and aids in informing risk of exposure to patients with disturbed intestinal epithelial barrier/inflammatory disorders such as IBD.

1. Background

Inflammatory bowel disease (IBD) is a chronic, non-specific inflammatory condition of the gastrointestinal tract (GI) that is associated with frequent relapse. The principal types of IBD are ulcerative colitis and Crohn's disease [1]. The incidence of IBD has gradually increased around the world in recent years [2]. It is well documented that abnormal immunological reactions caused by genetic and environmental factors contribute to the development of IBD [3]. However, the exact underlying mechanisms remain unclear and require further investigation.

With the development of nanoparticle technology, the safety of nanoparticles has garnered substantial attention among researchers. Graphene oxide (GO), a promising derivative of graphene, possesses a large surface area containing many surface functional groups, which renders it an attractive candidate for drug-delivery, cancer therapy, cell imaging, and tissue engineering [4–8]. A previous study reported that the market of GO in 2020 could reach $618 million [9]. Along with an increase of GO in production and application, there has been an increase in concern over the unintentional or occupational exposure of GO and its subsequent impact on human health [10]. Until now, multiple studies have provided evidence that GO could be directly cell permeable or readily engulfed by endocytosis into tissues and cells, leading to the induction of adverse effects [11–13]. For instance, inflammation responses in the lungs were

observed in mice after GO exposure [14–16]. Additionally, the potential *in vitro* toxicity of GO has been extensively studied and exposure to GO could cause a decrease in cell viability, alterations in the cell cycle, and apoptosis [17–19]. The intestinal tract is the primary site of interaction with nanomaterials; however, the intestinal epithelial barrier renders the uptake of nanoparticles complicated [20]. Although multiple studies have demonstrated the adverse impacts of GO on human health, only limited information on its effect on GI is available. In a systemic *in vivo* study conducted to detect the biodistribution of GO after intravenous and oral gavage, the results obtained suggested that the absorption of oral GO through the intestinal tract was ineffectual [15]. However, these data demonstrated that exposure to graphene family nanomaterials could alter intestinal barrier permeability by inducing apoptosis or changes in gut microbiota [21, 22]. Given above, the exact toxic effects of GO on the intestinal tract and which underlying molecular mechanisms are involved have not been systematically elucidated.

Intestinal epithelial cells (IECs) play a key role in maintaining the balance between the immune response and tissue homeostasis, especially as apoptosis of IECs contribute to the chronic intestinal inflammation of the gut, such as during IBD [23]. Previous studies have provided evidence that GO-induced cytotoxicity promoted apoptosis through the activation of various signaling pathways, such as p38-mitogen-activated protein kinase (MAPK) signaling cascade and extracellular signal-regulated kinase (ERK) signaling pathway [24, 25]. Adenosine monophosphate-activated protein kinase (AMPK), which is a conserved energy sensor, plays a crucial role in the antioxidant defense of cells and modulates cellular activities such as proliferation, cell cycle progression, and apoptosis [26]. Currently, the effects of GO on IEC apoptosis and the underlying mechanisms, such as the AMPK-related signaling pathway, remain unclear.

In the present study, we explored the potential toxicity of GO on the intestinal tract based on colitis induced by dextran sodium sulfate (DSS) and investigated the mechanism involved *in vitro*. Our study provides new insight into the pathogenesis of IBD, as it is related to environmental factors, and advances the current understanding of the risk of environmental exposure to GO.

2. Results

Characterization of GO

To characterize the GO used in this study, we used different microscopy techniques to observe the image of our GO samples. Representative atomic force microscopy (AFM) images of GO are shown in Fig. 1a. Most GO was found to exist in a single layer or a few layers with a thickness of ~ 1.0 nm and a lateral dimension ranging from 200 to 300 nm (Fig. 1b), which is consistent with the basic characteristics of GO nanosheets. As depicted in Fig. 1c, GO also showed a monolayer structure with sharp edges under transmission electron microscopy (TEM) observation. The original size distribution of GO in pure water is shown in Fig. 1d. Based on the Raman spectra results, we significantly observed two distinctive D and G peaks at 1344 cm^{-1} and 1602 cm^{-1}, respectively (Fig. 1e). Furthermore, we evaluated the stability and dispersity of GO using dynamic light scanning (DLS). As shown in Table 1, the average diameter of GO in

pure water, PBS, and culture medium was primarily in the range of 200–300 nm. However, GO showed aggregation in both PBS and culture medium over time, as characterized by gradually increased size, zeta-potential, and decreased polydispersity index (PDI), which indicated that GO may aggregate readily in the presence of salt or protein components.

Table 1
Stability and dispersity of GO nanoparticles in different media

GO	In water			In PBS			In RPMI-1640		
Time	Size (nm)	PDI	Zeta potential (mV)	Size (nm)	PDI	Zeta potential (mV)	Size (nm)	PDI	Zeta potential (mV)
12 h	159.9 ± 0.8	1.0	-14.4 ± 2.6	95.4 ± 0.8	1.0	-14.2	146.8 ± 0.2	1.0	-7.1
24 h	195.7 ± 0.8	1.0	-26.8	248.0 ± 1.4	1.0	-12.5	333.5 ± 0.8	1.0	-8.8
3 d	259.2 ± 0.7	1.0	-16.5 ± 4.0	255.6 ± 2.1	1.0	-17.0	321.4 ± 2.1	1.0	-16.4 ± 0.8
5 d	294.8 ± 0.6	1.0	-18.7	296.4 ± 0.9	1.0	-14.6 ± 0.9	370.3 ± 2.4	0.9	-9.4
7 d	311.8 ± 2.2	1.0	-17.7	342.9 ± 1.2	0.7	-17.1	1271 ± 3.9	0.5	-3.4

Oral administration of GO nanoparticles aggravated DSS-induced colitis

To evaluate whether GO exposure affects colitis in vivo, we studied four experimental groups of mice. From days 4 to 6, the weight of the mice in the DSS-WT and DSS-GO groups continuously decreased compared with that of the mice in the WT group. The DSS-induced colitis in mice was observed to be a spontaneous limited disease, and the mice typically had recovered from the weight loss after 7 days. However, after day 8, the DSS-GO group mice still showed a significant reduction in body weight compared with the DSS-WT group mice (Fig. 2b), and this was accompanied by obvious shortening of the colon (Fig. 2c, d). In addition, hematoxylin and eosin (H&E)-stained sections of colonic tissue showed severe inflammatory cell infiltration (Fig. 2e), and the total histological score indicated severe disruption of the mucosal epithelium in the DSS-GO group (Fig. 2f). Interestingly, mice that received GO in the absence of colitis showed no significant difference in weight, colon length, and histological scores from the corresponding parameters of mice in the WT group.

To further evaluate the inflammation response to GO in the intestinal tract, we next detected the expression of several important inflammatory cytokines, which play an important role in colitis. Our results showed that GO treatment in the absence of colitis did not cause obvious changes in IL-6, IL-17, and IFN-γ expression (Fig. 3a). However, the expression of these pro-inflammatory cytokines increased in

the DSS-WT and DSS-GO groups, while IL-10 expression decreased significantly (Fig. 3a). For further research on the effects of GO on intestinal inflammation, we finally measured intestinal apoptosis through TUNEL staining. A higher percent of apoptosis in the intestinal epithelium in the DSS-GO group was observed in comparison to the rate of apoptosis in the DSS-WT group intestinal epithelium, which may be the cause of the exacerbating colitis but still required further investigation on our part (Fig. 3b).

GO induced a dose- and time-dependent cytotoxicity in IECs

To explore the underlying mechanism behind GO aggravating colitis, we evaluated the biological activity of FHCs, a common human IEC model, following GO treatment. We first detected the localization of GO in FHCs by TEM and confocal microscopy. As depicted in Fig. 4a and b, GO was internalized and mainly distributed in the cytoplasm of FHCs. The potential toxic effects of GO on cell viability were then detected and we found that GO significantly decreased FHC viability in a dose- and time-dependent manner (Fig. 4c). Treatment with GO at a concentration of 50 μg/mL for 24 h resulted in approximately 50% cell death compared with the cell death rate of the control group.

Next, the cell membrane integrity was evaluated by LDH release. It is seen from Fig. 4d that the LDH release from FHCs significantly increased from 0 (control group) to more than 50% with 50 μg/mL GO treatment. In addition, LDH release increased with a longer duration of GO exposure, from 0 (no treatment) to 30% after 6 h of treatment and then to more than 50% after 24 h of treatment, which corresponds with the cell viability results. Based on the cell viability and LDH release results, we chose an appropriate concentration of GO (25 and 50 μg/mL) for further experiments.

In addition, the cell apoptosis induced by GO was also quantified by flow cytometry. As shown in Fig. 4e, the percentages of apoptotic cells were 25.32% in the control group, 39.5% among FHCs exposed to 25 μg/mL GO, and approximately 50% among FHCs exposed to 50 μg/mL GO.

GO induced mitochondrial dysfunction and reactive oxygen species (ROS) production in FHCs

The mitochondria play critical roles in the intrinsic apoptosis pathway and ROS production. In our examination of the effects of GO on mitochondrial function, we observed mitochondrial swelling and rupture after GO exposure (Fig. 5a). Next, we assessed the mitochondrial membrane potential (MMP), an important manifestation of early apoptosis, to evaluate mitochondrial function after exposure to GO. Following GO treatment, we observed a GO-induced decrease of MMP (Fig. 5b, c). Moreover, intracellular ROS generation was detected. As shown in Fig. 5d and e, GO enhanced the levels of intracellular ROS. For the purpose of revealing the potential mechanism responsible for cell apoptosis by GO, we detected the relevant apoptosis-related proteins, with a focus on cytochrome c (Cytc), Bax, Bcl-2 and cleaved caspase-3 (c-capase3). As shown using western blotting, GO treatment resulted in increased protein expression of Cytc, Bax, c-caspase3 and decreased protein expression of Bcl-2, consistent with the induction of apoptosis (Fig. 5f, g).

Taken together, our results demonstrated that GO induced apoptosis, as evidenced by mitochondrial damage, Cytc release and ROS overproduction. To investigate the association between Cytc and ROS, we used minocycline (MC, an inhibitor of Cytc) before GO treatment and found that protein expression of Cytc and intracellular ROS production were all reduced (Fig. 5h-j), which implied that GO-induced ROS generation resulted from mitochondrial dysfunction.

GO-induced apoptosis was regulated via ROS generation through the AMPK/p53 pathway in FHCs

Given that the AMPK pathway plays an important role in cellular apoptosis, we investigated the effect of GO treatment on the expression of proteins involved in the AMPK pathway, including AMPK, PI3K, AKT, and p53. The levels of phosphorylated AMPK and p53 was significantly increased after GO treatment for 24 h (Fig. 6a, b), whereas the levels of phosphorylated PI3K and AKT was not (Fig. 6c, d).

To further examine the relationship among GO-induced apoptosis, ROS overproduction, and AMPK/p53 activation, we treated FHCs with N-acetyl-L-cysteine (NAC), a ROS scavenger, and compound C (Com.C), a specific AMPK inhibitor, before incubation with GO. As shown in Fig. 7a and b, NAC significantly abrogated the GO-induced intracellular ROS accumulation. Additionally, flow cytometry showed significant reductions in GO-induced apoptosis after treatment of FHCs with NAC and Com.C, from 58–29.6% and 28.3%, respectively, compared with the control group (Fig. 7c). Moreover, pre-treating the FHCs with NAC and Com.C resulted in downregulated protein expression of c-caspase3 and Bax, and increased the protein expression of Bcl-2 (Fig. 7d, e). Finally, western blotting analysis showed that treatment with NAC and Com.C inhibited the phosophorylation of AMPKα (Thr172) and phosophorylated p53 in FHCs (Fig. 7f, g). These results suggest that GO-induced apoptosis is regulated via the ROS/AMPK/p53 signaling pathway.

3. Discussion

GO, a promising nanomaterial with a wide range of applications in biomedicine, has currently garnered tremendous research interest. Its extensive application means that the issue of potential GO toxicity worsens with increasing environmental exposure. The intestinal tract may be regarded as the primary targeted organ of nanomaterials due to its direct exposure to the external environment. Nevertheless, the current understanding of the mechanism behind GO toxicity on the intestinal tract is poorly understood. Only a few *in vivo* studies were performed to address the hazard of GO following oral exposure [27–29]. Damage to the intestinal mucosal barrier is a defining characteristic of chronic intestinal inflammatory disorders such as IBD [30]. Based on the present findings, we propose that there may be a close association between GO and chronic intestinal inflammation, which has not been studied/reported adequately. IBD has become a global health issue, its incidence continually increasing, particularly in countries undergoing increasing westernization, thus underscoring the vital role of environmental factors [31]. Herein, we hypothesize whether GO, a common environmental toxin, could negatively impact individuals with a defective intestinal barrier such as IBD patients. In the present study, we estimated the potential toxic effects of GO on a DSS-induced colitis mouse model.

The results obtained showed that acute oral administration of GO, with a particle size of 200–300 nm, at a dose of 60 mg/kg increased the extent of colitis, accompanied by obvious apoptosis in the intestinal mucosal epithelium. However, the GO-treated mice in the absence of colitis did not show any inflammation in the intestinal tract compared with the mice in the control group, which is in line with a previous study [15]. It is noteworthy that other nanoparticles, including titanium dioxide and silica nanoparticles, have also been showed to increase intestinal inflammation responses [27, 32, 33]. Taken together, we hypothesized that in a state of inflammation with a defective intestinal barrier, the absorption of nanoparticles is enhanced significantly, resulting in further inflammatory responses. These results suggest that GO may prove to be harmful in the light of pre-existing inflammatory disorders, such as IBD. Furthermore, *in vitro* experiments were performed to explore the potential mechanisms for the role of GO in colitis.

In our study, we focused on the cytotoxicity of GO in IECs, which plays an important role in the development of chronic inflammation including IBD. Currently, most *in vitro* studies have chosen to use a human colon adenocarcinoma cell (Caco-2) line as a model to explore the interaction of GO with IEC [34, 35]. However, evidence indicated that the uptake of GO was closely related to the differentiation status of Caco-2 [36]. Therefore, we chose the FHC cell line as an *in vitro* model in our study. Our data showed that the internalization of GO in the cytoplasm resulted in dose- and time-related alterations of cell viability, which correlate with the results of other studies in different cell models [17, 37, 38]. Considering the direct interaction of GO and the plasma membrane of IECs, we also observed obvious LDH release from IECs. It is commonly accepted that inflammatory responses, DNA damage, apoptosis, oxidative stress, necrosis, and autophagy are involved in the GO's toxicological mechanism [25, 39, 40]. Generally, the intracellular ROS generation, reflecting the oxidative stress status, has been reported to induce lipid peroxidation, protein inactivation, mitochondrial dysfunction, and eventually to activate apoptosis [41]. Based on our data, the destruction of mitochondrial structure, decrease in MMP, and increased level of intracellular ROS were observed in GO-treated IECs. We also observed obvious apoptosis in IECs following exposure to GO.

To the best of our knowledge, a number of apoptotic signals such as DNA damage and cell stress, in addition to nanomaterial exposure contribute to the activation of the Bcl-2 family proteins and promote permeabilization of the mitochondrial membrane, further resulting in the release of pro-apoptotic proteins such as cytochrome c and Bax. As a result of the formation of the apoptosome, caspase-9 and caspase-3 are activated and thus trigger apoptosis [42–44]. In our study, the GO-induced apoptosis is followed by the loss of MMP and the increase in intracellular ROS level, which indicated that the mitochondrial pathway may be primarily responsible for this effect. To investigate this, western blotting showed that GO exposure causes increased expression of Cytc, Bax, and c-caspase3, but decreased Bcl-2 expression. It has been suggested that Cytc is an essential molecular component of the electron transport chain, which promotes ROS generation [45]. In the present study, the inhibition of Cytc significantly prevented the intracellular ROS production induced by GO, which implies that GO-induced intracellular ROS accumulation results from mitochondrial dysfunction. Furthermore, prior studies have demonstrated that various signaling pathways are activated by ROS and numerous related genes such as MAPK, JNK and AMPK are involved in the apoptotic process [46–48]. Notably, AMPK plays an important role in the

regulation of apoptosis through modulating its downstream signaling molecules including p53, JNK, and mTOR [49–52]. To characterize the AMPK/p53 pathway involved, we measured the levels of AMPK and p53, as well as their phosphorylated forms. In the current study, we found that GO activates the AMPK/p53 pathway. Furthermore, we found that Com.C treatment leads to a significant decrease in apoptosis, which confirmed the crucial role of the AMPK/p53 pathway in GO-induced apoptosis. Cytosolic p53 has been demonstrated to translocate to the mitochondrial surface and directly interacts with Bcl-2 family proteins, further leading to the release of Bax and the activation of apoptosis [53]. We also observed an increased expression of Bcl-2 and reduced expression of Bax after pretreatment with Com.C. Moreover, the fact that NAC effectively inhibited the activation of AMPK suggests that ROS is an upstream molecule of AMPK activation, which is consistent with previous study [54].

As mentioned above, GO exposure to DSS-treated mice resulted in severe intestinal inflammation. Exposure of IECs to GO induced the loss of MMP and the generation of intracellular ROS. Subsequently, ROS activated the AMPK/p53 pathway to trigger apoptosis. This could be the main mechanism underlying the exacerbation of colitis by GO, which is illustrated in a schematic diagram (Fig. 8). However, concerning the underlying mechanisms responsible for GO exacerbation of colitis, our study only focused on ROS release and IECs apoptosis. There might be other mechanisms of apoptosis that could be involved and needs our further investigation. There might also be other mechanisms involved and needs our further investigation.

4. Conclusions

In summary, our findings demonstrated that the oral administration of GO exacerbated DSS-induced acute colitis via the activation of the ROS/AMPK/p53 signaling pathway to mediate apoptosis in IECs. Our study expands the understanding of GO toxicity in the GI and provides new insight into the biocompatibility of graphene materials, indicating that further research is needed. In addition, our findings suggested that individuals with a pre-existing intestinal inflammatory condition, such as IBD, must be cautious when unintentionally exposed to GO or its derivatives.

5. Materials And Methods

GO characterization

Commercially produced GO powder, purchased from Sigma-Aldrich (USA), was dispersed in pure water to prepare a stock solution (1 mg/mL). Prior to characterization and later experiments, the stock solution was sonicated for 2 h (40 kHz, power 99%). Prepared GO was characterized by AFM (Bruker, USA), TEM (Hitach, Japan) and Raman spectroscopy (Renishaw, UK). To acquire detailed information on its physicochemical properties, GO was dissolved in pure water, phosphate-buffered saline (PBS), and culture medium for 12 h, 24 h, 3 d, 5 d, and 7 d, and then the average diameter, zeta-potential, and PDI were analyzed by DLS (Malvern Instruments, UK).

Animal experimentation

Female C57Bl/6 mice (6–8 weeks old), purchased from the Animal Research Center of Southern Medical University (Guangzhou, China), were housed in a specific pathogen-free facility. The mice were divided into four groups (n = 5 per group): wild-type (WT) mice (WT control group), WT mice treated with GO (GO group), WT mice treated with DSS to induce colitis (DSS-WT group), and mice DSS-induced colitis that were exposed to GO (DSS-GO group). To generate the acute colitis model, female C57Bl/6 mice were administered 2.5% DSS (MP Biomedicals, USA) orally in drinking water for 5 days and then received normal drinking water for 3 days. Mice were exposed to GO separately via oral gavage at a dose of 60 mg/kg/day on second, fourth, sixth, and eighth day of the experiment. During the experiment, the mice were monitored daily to observe any occurrence of weight change, diarrhea, and rectal bleeding. A schematic representation of the animal protocol is provided in Fig. 2a.

H&E and TUNEL staining assay

The colon samples collected at the end of experiment were fixed in 4% paraformaldehyde, sectioned, and stained with H&E for examination by light microscopy. Histological scoring was carried out following a previously described system [55]. Apoptotic cells were stained with TUNEL for 1 h prior to observation under a fluorescence microscope (Nikon, Japan).

Detection of inflammatory cytokines

Total RNA from colon samples was extracted using TRIzol reagent (Gibco, USA) and quantified using the NanoDrop spectrophotometer (Thermo Fisher, USA). Quantitative real-time PCR (qPCR) was conducted and analyzed on LightCycler 480 (Roche, Switzerland). The inflammatory cytokine primers used are listed in Table 2.

Table 2
Primer sequences of IL-6, IL-10, IL-17 and IFN-γ used in the study

Gene name	Organism	Primer sequence
GAPDH	Mus musculus	GGGTCCCAGCTTAGGTTCAT
		TACGGCCAAATCCGTTCACA
IL-6	Mus musculus	TTCACAAGTCGGAGGCTTA
		CAAGTGCATCATCGTTGTTC
IL-10	Mus musculus	GGAAGAGAAACCAGGGAGA
		CCACAGTTTTCAGGGATGA
IL-17	Mus musculus	TTCACTTTCAGGGTCGAGA
		GGGGTTTCTTAGGGGTCA
IFN-γ	Mus musculus	ACTGGCAAAAGGATGGTG
		GTTGCTGATGGCCTGATT

Cell culture

Human IEC line FHCs were purchased from ATCC and maintained in complete RPMI-1640 (Gibco, USA) culture medium. FHCs were incubated with different concentrations of GO (0, 25, and 50 μg/mL) in the presence or absence of 100 μM minocycline (MC; Selleck, USA), 400 μM N-acetyl-L-cysteine (NAC; MCE, USA), or 10 μM Compound C (Com.C; MCE, USA).

Cell viability and membrane integrity assay in vitro

The Cell Counting Kit-8 assay (Dojingdo, Japan) and lactic dehydrogenase (LDH) assay were performed to evaluate the cell viability and cell membrane integrity, respectively. FHCs were exposed to GO at different concentrations (0, 10, 25, 50, 100, and 200 μg/mL) for 24 h or incubated with 0, 25 and 50 μg/mL GO for 6, 12 and 24 h. The optical density of each well at 450 nm (for Cell Counting Kit-8 tests) or 490 nm (for LDH test) was read by a microplate reader (Molecular Devices, USA).

Confocal microscope observation of GO uptake

Using a previously described method, the prepared GO suspension was mixed with fluorescein isothiocyanate (FITC)-conjugated bovine serum albumin (BSA, Bioss Inc, China) at a mass ratio of 1:1 and incubated overnight at 37°C in the dark [56]. The mixture was centrifuged at 12000 x *g* for 30 min at 4°C and washed briefly with PBS. Then, the pellet was resuspended in culture medium and added to cultures of FHCs. At the end of the treatment, the cells were washed with PBS, fixed with 4%

paraformaldehyde, and followed by 0.1% Triton X-100 permeabilization and nuclear staining. Finally, the samples were observed under a confocal microscope (Olympus, Japan).

TEM observations of GO uptake and mitochondrial structure

After the samples were treated as indicated, FHCs were fixed in 3% glutaraldehyde, post-fixed in osmium tetroxide, dehydrated in ethanol, and then polymerized using epoxy resin. GO uptake as well as the intracellular mitochondrial structure was observed *via* TEM (Hitachi, Japan).

Cell apoptosis assay

After incubation of FHCs in the presence or absence of GO for 24 h, cells were harvested and washed with PBS. After centrifugation, the cell pellet was suspended in 400 μL of Binding buffer to achieve a cell density of 1×10^6 cells/mL. The sample solution was then incubated with 5 μL Annexin V-FITC (Beyotime, China)for 15 min in the dark followed by an additional incubation with 10 μL propidium iodide (Invitrogen, USA) for 5 min. Apoptotic cells were detected by flow cytometry.

Flow Cytometry

Mitochondrial membrane potential (MMP) measurement

For MMP measurement, FHCs were treated with GO at concentrations of 0, 25, and 50 μg/mL, and cells treated with 10 μg/mL lipopolysaccharide (LPS; Sigma-Aldrich, USA) served as the positive control group. After exposure to GO or LPS, cells were incubated with JC-1 buffer mixture solution (Beyotime, China) according to the manufacturer's instructions. Fluorescence microscopy and flow cytometry (BD Biosciences, USA) were used to measure the ratio of red/green fluorescence, which reflected the relative value of MMP.

Reactive oxygen species (ROS) generation assay

Intracellular ROS production was measured using the DCFHDA assay kit (Beyotime, China). After treatment with GO in the presence or absence of NAC and Com.C, FHCs were harvested by centrifugation and stained with DCFHDA for 30 min in the dark at room temperature. The fluorescence intensity was analyzed by fluorescence microscopy and flow cytometry.

Western blotting analysis

A total of 30 μg of protein was separated by 10% SDS-PAGE and transferred to a PVDF membrane, which was then blocked with 5% w/v BSA. Membranes were probed with the indicated primary antibodies including rabbit polyclonal antibodies against cytochrome c (Cytc), cleaved caspase-3 (c-caspase3), Bcl-2, phosphorylated (p)-AMPKα (Thr172), p-PI3K, PI3K, p-Akt, Akt, p-p53, and p53 (Cell Signaling Technology, USA) along with mouse monoclonal antibodies to Bax and AMPK (Proteintech, China) and GAPDH were used to normalize protein expression. Appropriate secondary antibodies conjugated to

horseradish-peroxidase (HRP) were then added and incubated for 1 h. The antigen–antibody complex was detected using an enhanced chemiluminescence reagent (Millipore, USA). The gray intensity of the bands on the western blotting was analyzed using ImageJ software (NIH, Bethesda, USA).

Statistical analysis

The experimental data are presented as mean ± standard error of the mean (SEM). Differences among the data for the different groups were analyzed by one-way ANOVA. *P*-values less than 0.05 and 0.01 were considered significant, as indicated.

Abbreviations

GO: graphene oxide; IBD: inflammatory bowel disease; IEC: intestinal epithelial cell; DSS: dextran sulfate sodium; ROS: reactive oxygen species; AMPK: AMP-activated protein kinase; AFM: atomic force microscopy; TEM: transmission electron microscopy; DLS: dynamic light scanning; PDI: polydispersity index; MC: minocycline; NAC:N-acetyl-L-cysteine; Com.C: compound C; FITC: fluorescein isothiocyanate; BSA: bovine serum albumin; LDH: Lactic dehydrogenase; c-caspase3: cleaved caspase-3; MMP: mitochondrial membrane potential; LPS: lipopolysaccharide; Cytc: cytochrome c; H&E: hematoxylin and eosin; qPCR: quantitative real-time PCR; p: phosphorylated; SEM: standard error of the mean.

Declarations

Ethics approval

The experimental protocols were approved by the Southern Medical University Ethics and Experimentation of Committee (grant number L2016189).

Consent for publication

All authors agree to be published.

Availability of data and materials

The datasets used or analyzed during the current study are available from the corresponding author upon reasonable request.

Competing interests

The authors report no conflicts of interests in this work.

Funding

This work was supported by National Natural Science Foundation of China (grant number 81572938).

Authors' contributions

Siliang Liu, Angao Xu, and Yue Xie: animal and cell experiments, drafting the manuscript, data acquisition, and analysis. Zhipeng and Meiling Sun: material and technological support. Yanfei Gao and Hua Mao: data arrangement and analysis, study concept, and supervision; Xinying Wang: manuscript revision, study concept, design, supervision, and funding.

Acknowledgements

The authors thank to the Guangdong Provincial Key Laboratory of Gastroenterology, Department of Gastroenterology, Nanfang Hospital, Southern Medical University, Guangzhou, Guangdong, China. Moreover, we would like to thank Editage (www.editage.cn) for their writing support on this manuscript.

References

1. Baumgart DC, Sandborn WJ. Inflammatory bowel disease: clinical aspects and established and evolving therapies. Lancet (London, England). 2007;369:1641-57.
2. Malekzadeh MM, Vahedi H, Gohari K, Mehdipour P, Sepanlou SG, Ebrahimi Daryani N, et al. Emerging Epidemic of Inflammatory Bowel Disease in a Middle Income Country: A Nation-wide Study from Iran. Arch Iran Med. 2016;19:2-15.
3. Lakatos L, Mester G, Erdelyi Z, Balogh M, Szipocs I, Kamaras G, et al. Striking elevation in incidence and prevalence of inflammatory bowel disease in a province of western Hungary between 1977-2001. World J Gastroenterol. 2004;10:404-9.
4. Sun X, Liu Z, Welsher K, Robinson JT, Goodwin A, Zaric S, et al. Nano-Graphene Oxide for Cellular Imaging and Drug Delivery. Nano research. 2008;1:203-12.
5. Langer R, Vacanti J. Advances in tissue engineering. J Pediatr Surg. 2016;51:8-12.
6. Yao C, Tu Y, Ding L, Li C, Wang J, Fang H, et al. Tumor Cell-Specific Nuclear Targeting of Functionalized Graphene Quantum Dots In Vivo. Bioconjug Chem. 2017;28:2608-19.
7. Yin F, Hu K, Chen Y, Yu M, Wang D, Wang Q, et al. SiRNA Delivery with PEGylated Graphene Oxide Nanosheets for Combined Photothermal and Genetherapy for Pancreatic Cancer. Theranostics. 2017;7:1133-48.
8. Hussien NA, Isiklan N, Turk M. Pectin-conjugated magnetic graphene oxide nanohybrid as a novel drug carrier for paclitaxel delivery. Artif Cells Nanomed Biotechnol. 2018;46:264-73.
9. Ahmed F, Rodrigues DF. Investigation of acute effects of graphene oxide on wastewater microbial community: a case study. J Hazard Mater. 2013;256-257:33-9.
10. Pelin M, Sosa S, Prato M, Tubaro A. Occupational exposure to graphene based nanomaterials: risk assessment. Nanoscale. 2018;10:15894-903.
11. Li J, Zhang X, Jiang J, Wang Y, Jiang H, Zhang J, et al. Systematic assessment of the toxicity and potential mechanism of graphene derivatives in vitro and in vivo. Toxicol Sci. 2019;167(1):269-281.

12. Kersting D, Fasbender S, Pilch R, Kurth J, Franken A, Ludescher M, et al. From in vitro to ex vivo: subcellular localization and uptake of graphene quantum dots into solid tumors. Nanotechnology. 2019;30:395101.
13. Krajnak K, Waugh S, Stefaniak A, Schwegler-Berry D, Roach K, Barger M, et al. Exposure to graphene nanoparticles induces changes in measures of vascular/renal function in a load and form-dependent manner in mice. J Toxicol Environ Health A. 2019;82:711-26.
14. Duch MC, Budinger GR, Liang YT, Soberanes S, Urich D, Chiarella SE, et al. Minimizing oxidation and stable nanoscale dispersion improves the biocompatibility of graphene in the lung. Nano Lett. 2011;11:5201-7.
15. Yang K, Gong H, Shi X, Wan J, Zhang Y, Liu Z. In vivo biodistribution and toxicology of functionalized nano-graphene oxide in mice after oral and intraperitoneal administration. 2013;34:2787-95.
16. Park EJ, Lee SJ, Lee K, Choi YC, Lee BS, Lee GH, et al. Pulmonary persistence of graphene nanoplatelets may disturb physiological and immunological homeostasis. J Appl Toxicol. 2017;37:296-309.
17. Feng X, Chen L, Guo W, Zhang Y, Lai X, Shao L, et al. Graphene oxide induces p62/SQSTM-dependent apoptosis through the impairment of autophagic flux and lysosomal dysfunction in PC12 cells. Acta Biomater. 2018;81:278-292..
18. Arbo MD, Altknecht LF, Cattani S, Braga WV, Peruzzi CP, Cestonaro LV, et al. In vitro cardiotoxicity evaluation of graphene oxide. Mutat Res. 2019;841:8-13.
19. Gurunathan S, Arsalan Iqbal M, Qasim M, Hyeok Park C, Yoo H, Ho Hwang J, et al. Evaluation of Graphene Oxide Induced Cellular Toxicity and Transcriptome Analysis in Human Embryonic Kidney Cells. Nanomaterials. 2019;9(7):969..
20. Neves AR, Queiroz JF, Costa Lima SA, Figueiredo F, Fernandes R, Reis S. Cellular uptake and transcytosis of lipid-based nanoparticles across the intestinal barrier: Relevance for oral drug delivery. J Colloid Interface Sci. 2016;463:258-65.
21. Wu Q, Yin L, Li X, Tang M, Zhang T, Wang D. Contributions of altered permeability of intestinal barrier and defecation behavior to toxicity formation from graphene oxide in nematode Caenorhabditis elegans. Nanoscale. 2013;5:9934-43.
22. Chen H, Zhao R, Wang B, Zheng L, Ouyang H, Wang H, et al. Acute Oral Administration of Single-Walled Carbon Nanotubes Increases Intestinal Permeability and Inflammatory Responses: Association with the Changes in Gut Microbiota in Mice. Adv Healthc Mater. 2018;7:e1701313.
23. Neurath MF, Travis SP. Mucosal healing in inflammatory bowel diseases: a systematic review. Gut. 2012;61:1619-35.
24. Zhao Y, Zhi L, Wu Q, Yu Y, Sun Q, Wang D. p38 MAPK-SKN-1/Nrf signaling cascade is required for intestinal barrier against graphene oxide toxicity in Caenorhabditis elegans. 2016;10:1469-79.
25. Kang Y, Liu J, Wu J, Yin Q, Liang H, Chen A, et al. Graphene oxide and reduced graphene oxide induced neural pheochromocytoma-derived PC12 cell lines apoptosis and cell cycle alterations via the ERK signaling pathways. Int J Nanomedicine. 2017;12:5501-10.

26. Afrin M, Arumugam S, Rahman M, Karuppagounder V, Sreedhar R, Harima M, et al. Le Carbone, a charcoal supplement, modulates DSS-induced acute colitis in mice through activation of AMPKα and downregulation of STAT3 and caspase 3 dependent apoptotic pathways. Int Immunopharmacol. 2017;43:70-8.
27. Fu C, Liu T, Li L, Liu H, Liang Q, Meng X. Effects of graphene oxide on the development of offspring mice in lactation period. Biomaterials. 2015;40:23-31.
28. Zhang D, Zhang Z, Liu Y, Chu M, Yang C, Li W, et al. The short- and long-term effects of orally administered high-dose reduced graphene oxide nanosheets on mouse behaviors. Biomaterials. 2015;68:100-13.
29. Patlolla AK, Rondalph J, Tchounwou PB. Biochemical and Histopathological Evaluation of Graphene Oxide in Sprague-Dawley Rats. Austin J Environ Toxicol. 2017;3(1):1021.
30. Shen L, Turner JR. Role of epithelial cells in initiation and propagation of intestinal inflammation. Eliminating the static: tight junction dynamics exposed. Am J Physiol Gastrointest Liver Physiol. 2006;290:G577-82.
31. Kaplan GG, Ng SC. Understanding and Preventing the Global Increase of Inflammatory Bowel Disease. Gastroenterology. 2017;152:313-21.e2.
32. Ruiz PA, Moron B, Becker HM, Lang S, Atrott K, Spalinger MR, et al. Titanium dioxide nanoparticles exacerbate DSS-induced colitis: role of the NLRP3 inflammasome. 2017;66:1216-24.
33. Mu W, Wang Y, Huang C, Fu Y, Li J, Wang H, et al. Effect of Long-Term Intake of Dietary Titanium Dioxide Nanoparticles on Intestine Inflammation in Mice. J Agric Food Chem. 2019;67:9382-9.
34. Kucki M, Rupper P, Sarrieu C, Melucci M, Treossi E, Schwarz A, et al. Interaction of graphene-related materials with human intestinal cells: an in vitro approach. 2016;8:8749-60.
35. Guarnieri D, Sanchez-Moreno P, Del Rio Castillo AE, Bonaccorso F, Gatto F, Bardi G, et al. Biotransformation and Biological Interaction of Graphene and Graphene Oxide during Simulated Oral Ingestion. Small. 2018;14:e1800227.
36. Kucki M, Diener L, Bohmer N, Hirsch C, Krug HF, Palermo V, et al. Uptake of label-free graphene oxide by Caco-2 cells is dependent on the cell differentiation status. J Nanobiotechnology. 2017;15:46.
37. Frontiñán-Rubio J, Gómez M, Martín C, González-Domínguez J, Durán-Prado M, Vázquez E. Differential effects of graphene materials on the metabolism and function of human skin cells. Nanoscale. 2018;10:11604-15.
38. Wei M, Fu Z, Wang C, Zheng W, Li S, Le W. Graphene Oxide Nanocolloids Induce Autophagy-Lysosome Dysfunction in Mouse Embryonic Stem Cells. J Biomed Nanotechnol. 2019;15:340-51.
39. Vranic S, Rodrigues AF. Live Imaging of Label-Free Graphene Oxide Reveals Critical Factors Causing Oxidative-Stress-Mediated Cellular Responses. ACS Nano. 2018;12(2):1373-1389.
40. Gurunathan S, Kang MH, Jeyaraj M, Kim JH. Differential Cytotoxicity of Different Sizes of Graphene Oxide Nanoparticles in Leydig (TM3) and Sertoli (TM4) Cells. Nanomaterials (Basel). 2019;9(2):139.

41. Thubagere A, Reinhard BM. Nanoparticle-induced apoptosis propagates through hydrogen-peroxide-mediated bystander killing: insights from a human intestinal epithelium in vitro model. ACS nano. 2010;4:3611-22.
42. Cheng WC, Leach KM, Hardwick JM. Mitochondrial death pathways in yeast and mammalian cells. Biochim Biophys Acta. 2008;1783:1272-9.
43. Brenner D, Mak TW. Mitochondrial cell death effectors. Curr Opin Cell Biol. 2009;21:871-7.
44. Brunelle JK, Letai A. Control of mitochondrial apoptosis by the Bcl-2 family. J Cell Sci. 2009;122:437-41.
45. Krysko DV, Agostinis P, Krysko O, Garg AD, Bachert C, Lambrecht BN, et al. Emerging role of damage-associated molecular patterns derived from mitochondria in inflammation. Trends Immunol. 2011;32:157-64.
46. X S, Z S, Q Y, F S, J P, J M, et al. Vitamin C kills thyroid cancer cells through ROS-dependent inhibition of MAPK/ERK and PI3K/AKT pathways via distinct mechanisms. 2019;9:4461-73.
47. C W, P L, J X, C Z, J L, L S, et al. Cholesterol Enhances Colorectal Cancer Progression via ROS Elevation and MAPK Signaling Pathway Activation.Cell Physiol Biochem. 2017;42:729-42.
48. Z Y, H XB, L YJ, D SM, W ZW, H WM, et al. ROS signaling under metabolic stress: cross-talk between AMPK and AKT pathway. Mol Cancer. 2017;16:79.
49. M XJ, H JG, W Z, H Y, R S, H JN, et al. The protective effects of maltol on cisplatin-induced nephrotoxicity through the AMPK-mediated PI3K/Akt and p53 signaling pathways. Sci Rep. 2018;8:15922.
50. H B, X Y, S F, L XS, H J, T MB, et al. Metformin-induced activation of AMPK inhibits the proliferation and migration of human aortic smooth muscle cells through upregulation of p53 and IFI16. Int J Mol Med. 2018;41:1365-76.
51. C X, L X, Z WY, H J, X B, W ZH, et al. Activation of AMPK inhibits inflammatory response during hypoxia and reoxygenation through modulating JNK-mediated NF-κB pathway. 2018;83:256-70.
52. L C, D YC, W LB, X GB, Y Q, T XF, et al. Ginsenoside metabolite compound K induces apoptosis and autophagy in non-small cell lung cancer cells via AMPK-mTOR and JNK pathways. Biochem Cell Biol. 2019;97:406-14.
53. Luna-Vargas MP, Chipuk JE. The deadly landscape of pro-apoptotic BCL-2 proteins in the outer mitochondrial membrane. Febs j. 2016;283:2676-89.
54. Chen MB, Zhang Y, Wei MX, Shen W, Wu XY, Yao C, et al. Activation of AMP-activated protein kinase (AMPK) mediates plumbagin-induced apoptosis and growth inhibition in cultured human colon cancer cells. Cell Signal. 2013;25:1993-2002.
55. Dann SM, Spehlmann ME, Hammond DC, Iimura M, Hase K, Choi LJ, et al. IL-6-dependent mucosal protection prevents establishment of a microbial niche for attaching/effacing lesion-forming enteric bacterial pathogens. J Immunol. 2008;180:6816-26.

56. Mu Q, Su G, Li L, Gilbertson BO, Yu LH, Zhang Q, et al. Size-dependent cell uptake of protein-coated graphene oxide nanosheets. ACS Appl Mater Interfaces. 2012;4(4):2259-66.

Figures

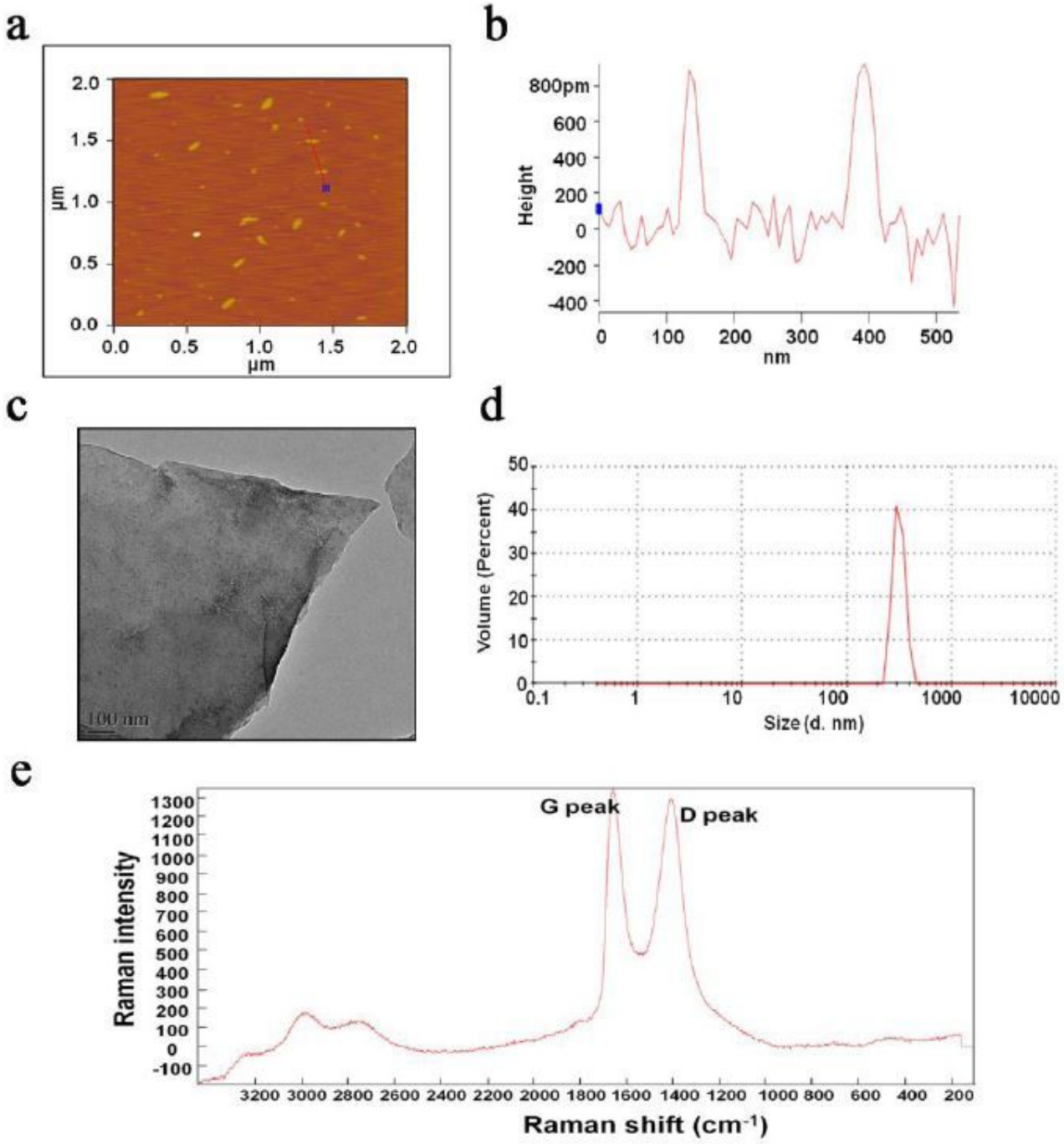

Figure 1

The characterization of GO. (a and b) Representative AFM image of GO. (c) Representative TEM image of GO. Scale bar: 100 nm. (d) The original image of size distribution of GO in pure water by DLS. (e) Raman spectroscopy of GO nanosheets. GO: graphene oxide; AFM: atomic force microscopy; TEM: transmission electron microscopy

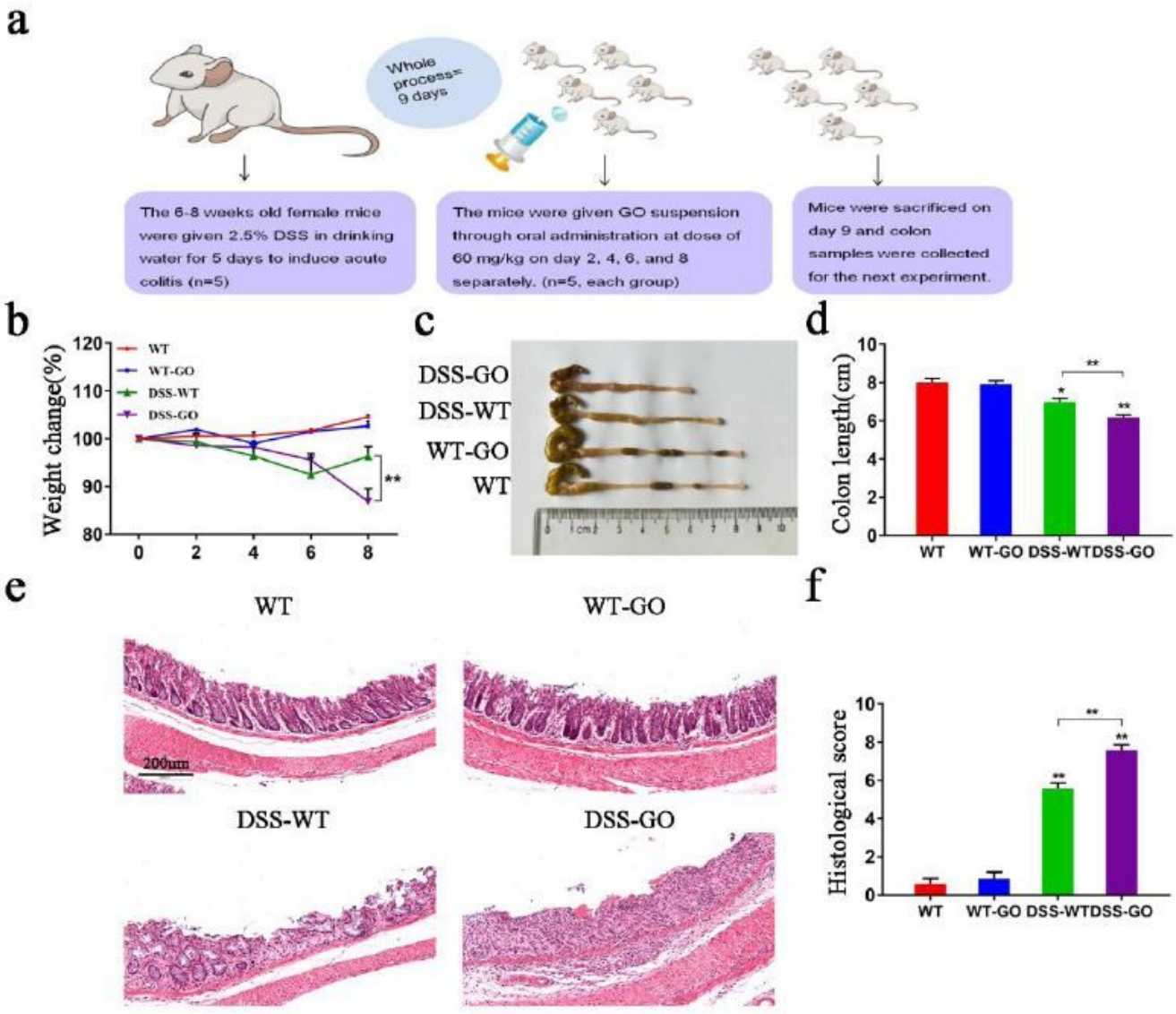

Figure 2

Administration of GO aggravated the DSS-induced colitis in mice. (a) Schematic illustrations of experiments on the intestinal toxicity of mice after repeated oral exposure with GO. (b) Weight changes and (c and d) colon length were measured. Body weight was presented as the percentage of the initial weight (at day 0). (e) Representative H&E images of colon tissues. Scale bar: 200 μm. (f) The total histological score was calculated as the sum of the score for epithelial damage and the infiltration score. Data are presented as mean ± SEM from three independent experiments in all analyses. *P<0.05,

**P<0.01. GO: graphene oxide; DSS: dextran sodium sulfate; H&E: hematoxylin and eosin; SEM: standard error of the mean

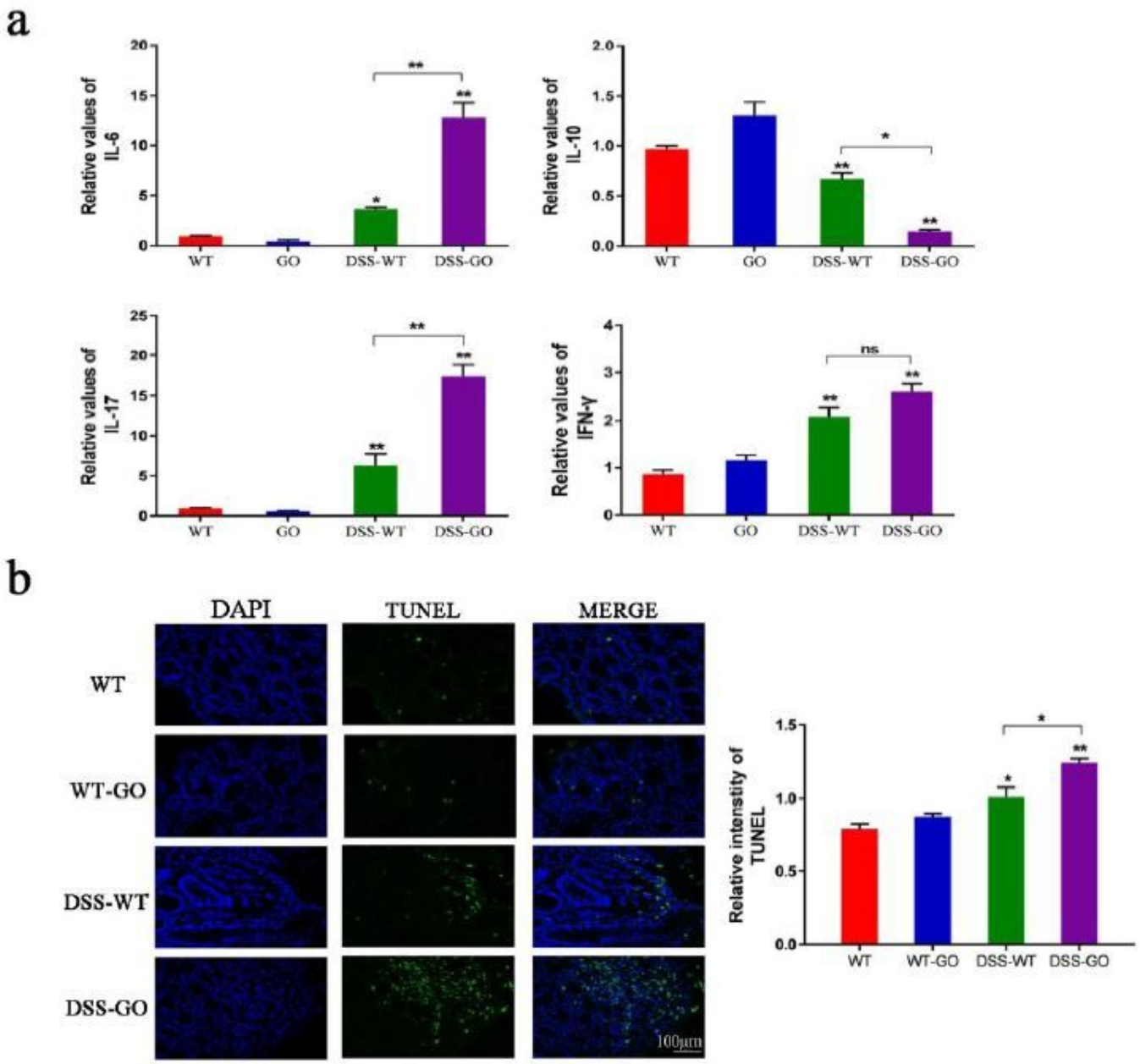

Figure 3

GO induced the production of pro-inflammatory cytokines and obvious apoptosis in DSS-induced colitis mice. (a) The relative levels of IL-6, IL-10, IL-17, and IFN-γ in mice were detected through qPCR. (b) The apoptosis in intestinal tract was detected by TUNEL assay. Scale bar: 100 μm. *P<0.05, **P<0.01. GO: graphene oxide; DSS: dextran sodium sulfate; qPCR: quantitative real-time PCR

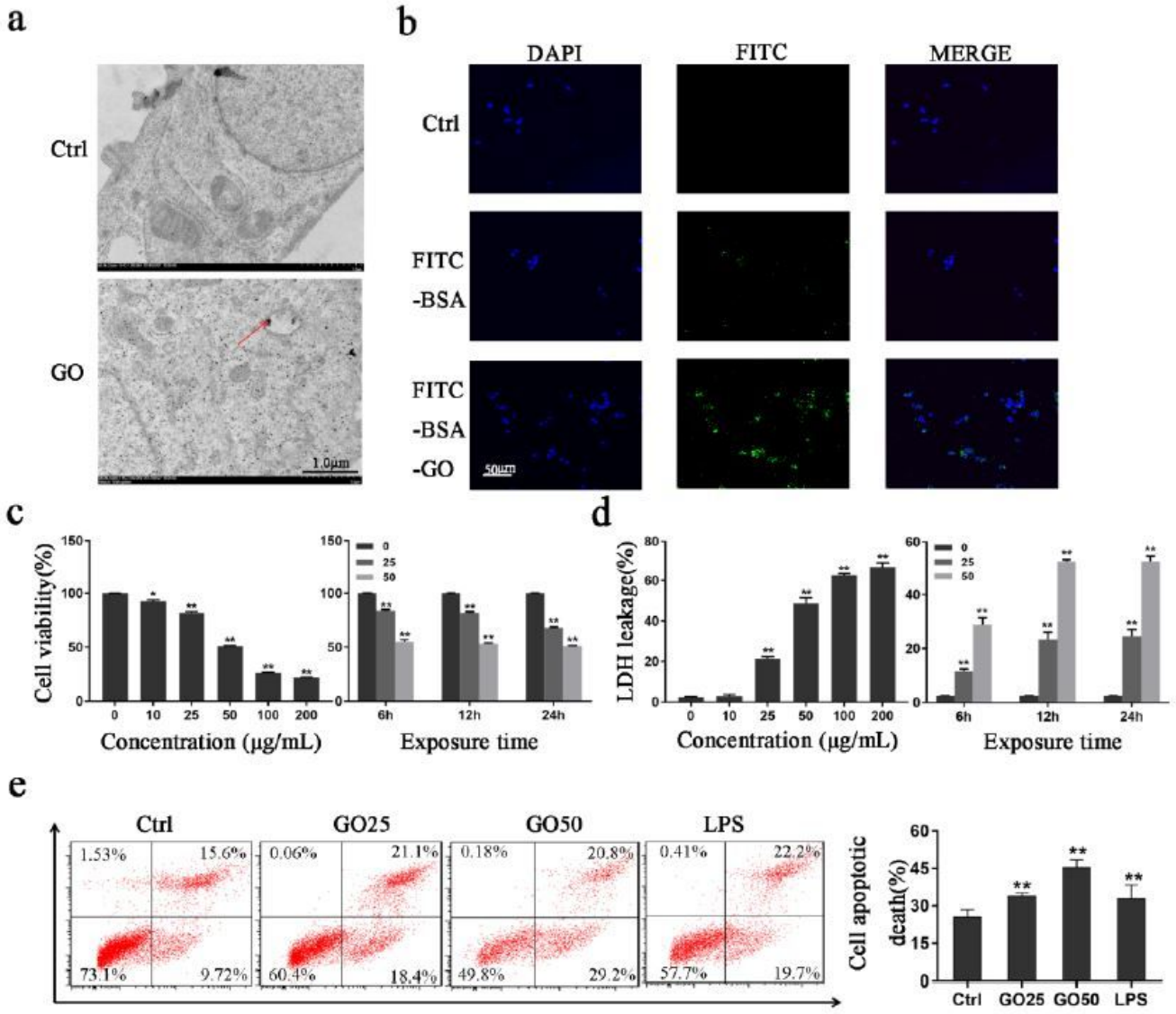

Figure 4

GO induced a dose- and time-dependent cytotoxicity in FHCs. (a and b) TEM and confocal microscopy observation of GO in FHCs following 50 μg/mL GO treatment for 24 h. The red arrows indicate the GO accumulation in cytoplasm. Scale bar: 1 μm and 50μm. (c and d) Relative cell viability and LDH release in cultured FHCs incubated with GO at different concentrations (0, 10, 25, 50, 100, or 200 μg/mL) for 24 h, or 25 and 50 μg/mL GO for 6, 12, and 24 h. (e) The apoptosis of FHCs incubated with culture medium containing GO (0, 25 or 50μg/mL) for 24 h, while LPS treatment served as the positive control. Apoptotic cell death was expressed by the sum of the percentage of early apoptotic cells and late apoptotic cells. *P<0.05, **P<0.01. GO: graphene oxide; TEM: transmission electron microscopy; LDH: lactic dehydrogenase; LPS: lipopolysaccharide

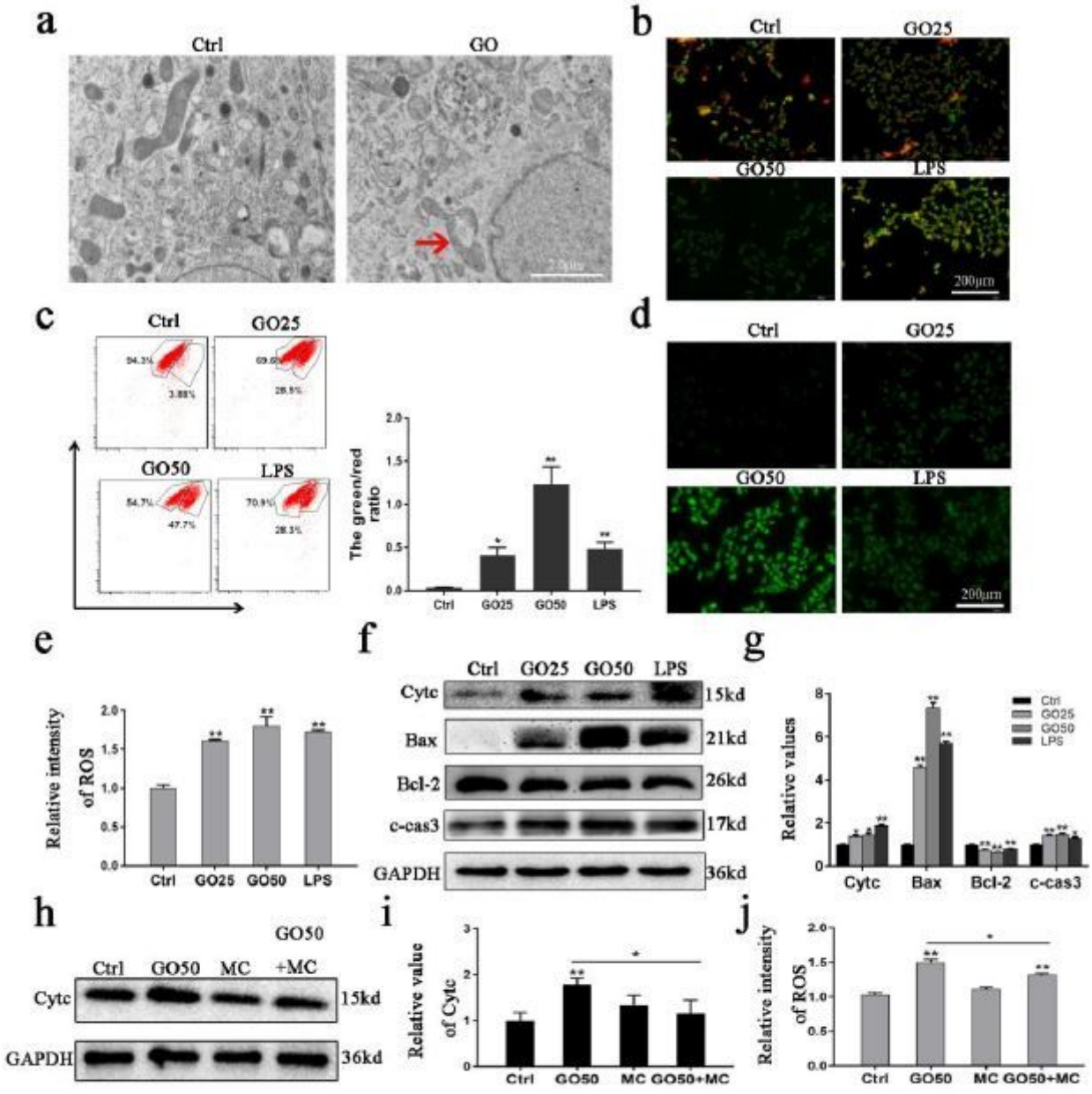

Figure 5

GO induced mitochondrial dysfunction and ROS production in FHCs. (a) TEM observation of mitochondrial structure in FHCs following exposure to 50 μg/mL GO treatment. Scale bar: 2.0 μm. (b and c). The MMP was analyzed via fluorescence microscopy and flow cytometry after GO or LPS treatment as indicated. Scale bar: 200 μm. (d and e) Fluorescence microscopy and flow cytometry were performed to measure intracellular ROS production. Scale bar: 200 μm. (f and g) The levels of apoptosis-related proteins Cytc, Bax, Bcl-2, and c-caspase3 using western blotting. (h and i) Western blotting of the expression of Cytc after incubation with GO in the presence of absence of MC. (j) The intracellular ROS production after GO treatment in the absence or presence of MC, as measured by flow cytometry. *P<0.05,

**P<0.01. GO: graphene oxide; ROS: reactive oxygen species; TEM: transmission electron microscopy; MMP: mitochondrial membrane potential; LPS: lipopolysaccharide; Cytc: cytochrome c; c-caspase3: cleaved caspase-3; MC: minocycline

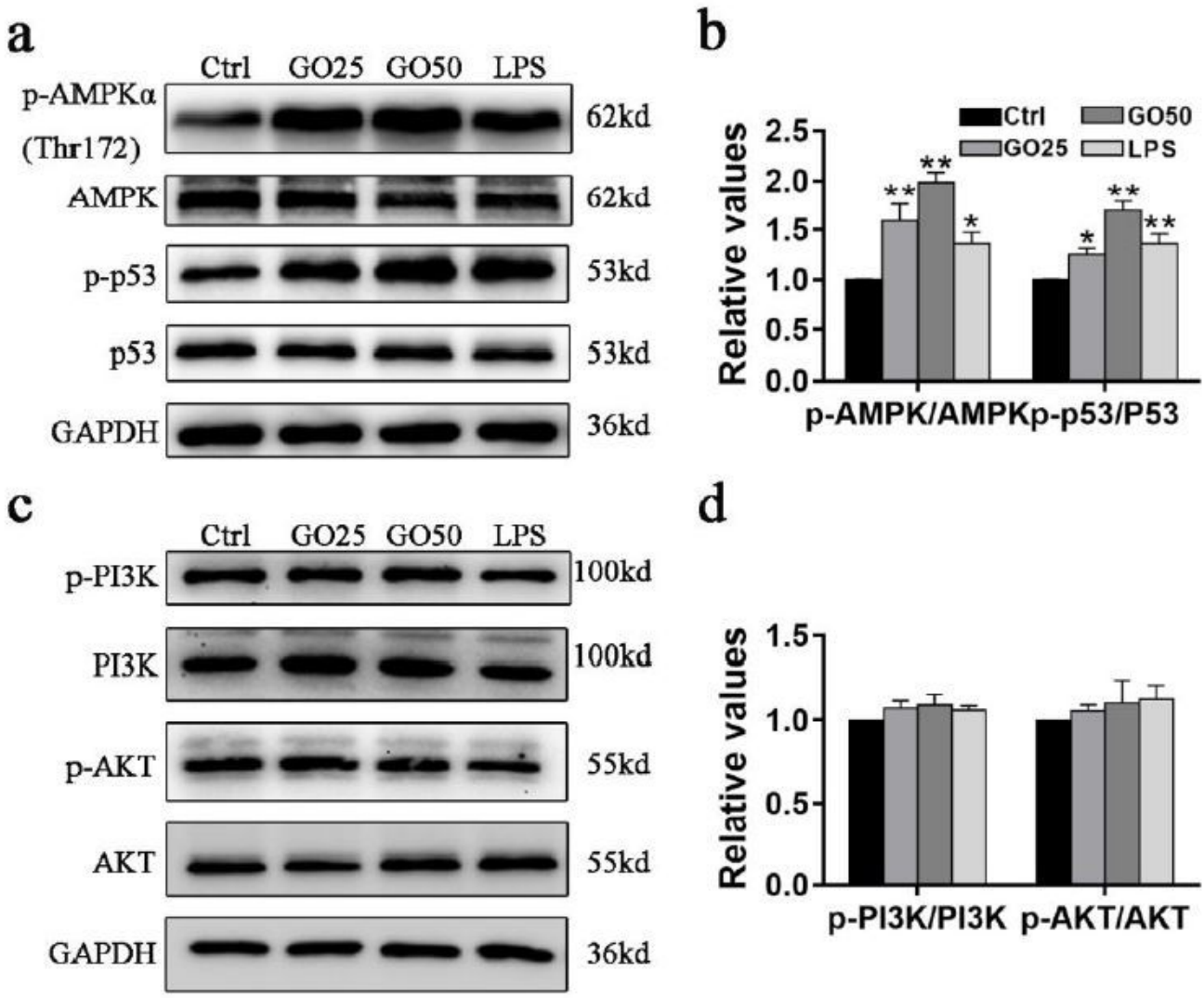

Figure 6

GO activated the AMPK/p53 signaling pathway in FHCs. FHCs were treated with 0, 25, or 50 μg/mL GO for 24 h, and LPS served as the positive control group. (a to d) Cell lysates were subjected to western blotting to analyze the expression of p-AMPK (Thr172), AMPK, p-p53, p53, p-PI3K, PI3K, p-AKT, and AKT. Changes in the levels of the phosphorylated proteins were quantified after normalization against the corresponding pan proteins. *P<0.05, **P<0.01 compared with the control group. GO: graphene oxide; AMPK: adenosine monophosphate-activated protein kinase; LPS: lipopolysaccharide; p: phosphorylated

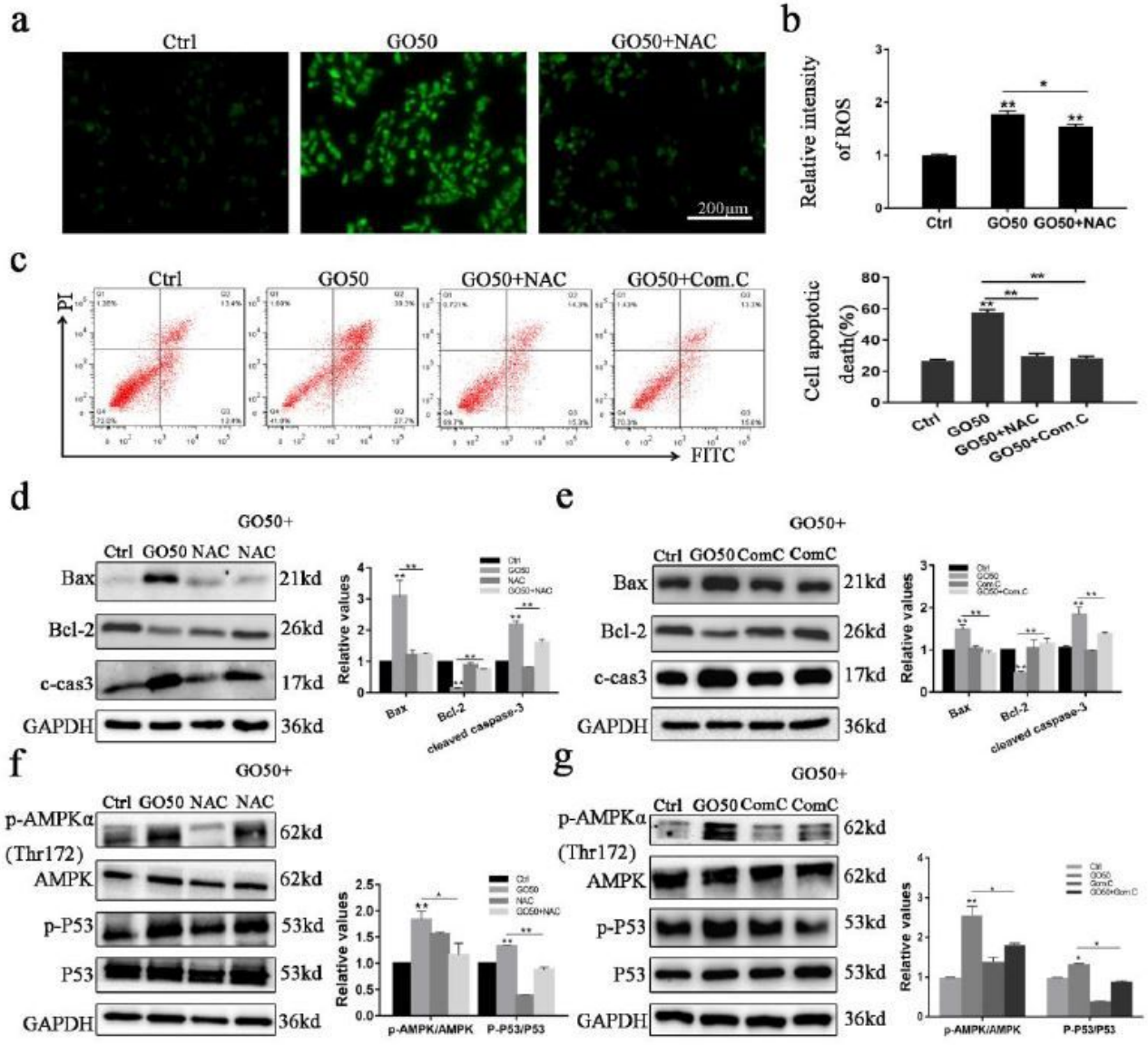

Figure 7

GO-induced apoptosis in FHCs was regulated via the ROS/AMPK/p53 pathway. Cells were incubated with 50 μg/mL GO in the absence or presence of 400 μM NAC or 10 μM Com.C. (a and b) The intracellular ROS level was measured by DCFHDA detection through fluorescence microscopy and flow cytometry. Scale bar: 200 μm. (c) Flow cytometry was used to evaluate the apoptotic rate of FHCs after exposure to GO. (d and e) The relative expression of Bax, Bcl-2, and c-caspase3 was measured using western blotting. (f and g) The relative expression of AMPK/p53 signaling pathway-related proteins after GO treatment in the absence or presence of NAC or Com.C using western blotting. Changes in the levels of these proteins were quantified after normalization against GAPDH or AMPK and p53. *P<0.05, **P<0.01. GO: graphene oxide; ROS: reactive oxygen species; AMPK: adenosine monophosphate-activated protein kinase; c-caspase3: cleaved caspase-3; NAC: N-acetyl-L-cysteine; Com.C: compound C

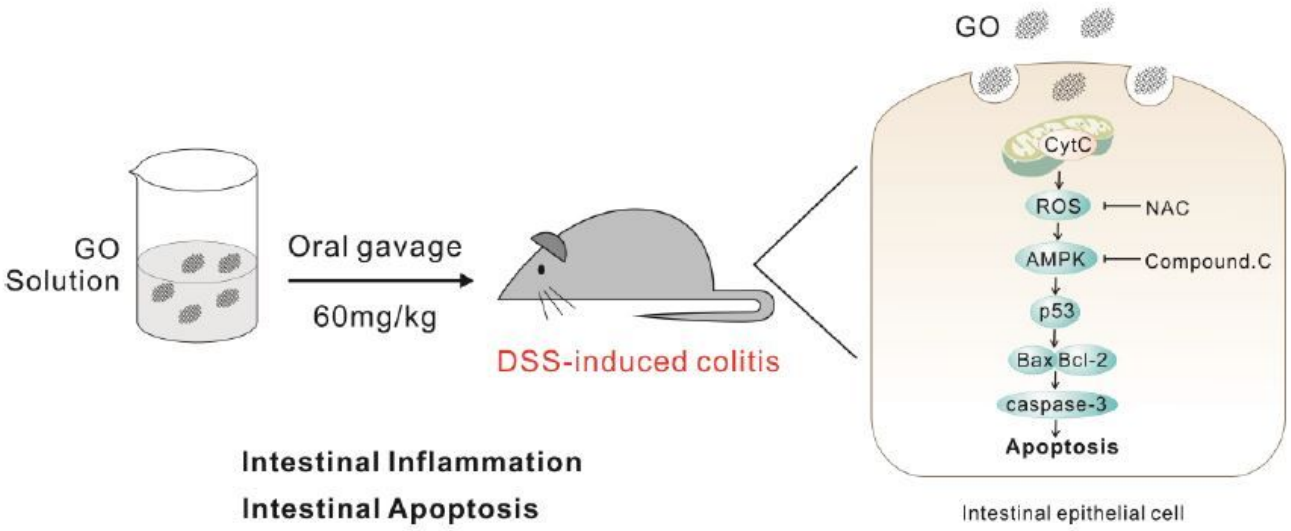

Figure 8

Schematic diagram of the effects of GO on IECs. GO exacerbates DSS-induced colitis through inducing apoptosis in IECs via activation of the ROS/AMPK/p53 signaling pathway, which could be inhibited by NAC and compound C. GO: graphene oxide; IECs: intestinal epithelial cells; DSS: dextran sodium sulfate; ROS: reactive oxygen species; AMPK: adenosine monophosphate-activated protein kinase; NAC: N-acetyl-L-cysteine